JOURNAL OF GEOPHYSICAL RESEARCH, VOL. ???, XXXX, DOI:10.1029/,

Potential vorticity and upstream control of the East Australian Current separation: a Lagrangian approach

S.L. Ypma[1,2.5], E. van Sebille[2,3,5], A.E. Kiss[4,5] and P. Spence[2,5]

Abstract. The East Australian Current (EAC) is the western boundary current flowing along the east coast of Australia separating from the coast at approximately 34°S. After the separation two main pathways can be distinguished, the eastward flowing Tasman Front and the extension of the EAC

---

[1]Institute for Marine and Atmospheric Research Utrecht, Utrecht University, Netherlands.

[2]Climate Change Research Centre, University of New South Wales, Sydney, New South Wales, Australia.

[3]Grantham Institute & Department of Physics, Imperial College London, London, United Kingdom.

[4]School of Physical, Environmental and Mathematical Sciences, University of New South Wales Canberra at the Australian Defence Force Academy, Australia.

[5]ARC Centre of Excellence for Climate System Science, University of New South Wales, Sydney, Australia.

flowing southwards. The area south of the separation latitude is eddy-rich, making the EAC region a variable and dynamic system. There have been several studies that explain the physical aspects of this separation of the EAC, addressing the importance of gradients in the wind stress curl, coastline curvature, bottom topography, forcing from westward propagating Rossby waves and potential vorticity. There is however no consensus on which process is dominant in determining the exact separation latitude and little is known of the properties of the water masses that separate at the bifurcation of the EAC. This paper presents new insights from the Lagrangian perspective, where the water masses that veer east and those that continue south are tracked in an eddy-permitting numerical model. The Lagrangian approach is used to compute the transport along the two pathways, where a 1:3 ratio between transport in the extension of the EAC and transport in the Tasman Front is found. The results show that the 'fate' of the particles is to first order already determined by the particles distribution within the EAC current upstream of the separation latitude, where 83% of the particles following the extension of the EAC originate from a depth between 640m and 1000m and 72% of the particles following the Tasman Front originate from the top 640m depth. The separation and pathways are controlled by the structure of the isopycnals in this region. Analysis of anomalies in potential vorticity show that in the region where the two water masses overlap, the fate of the water depends on the presence of anticyclonic eddies that push the isopycnals down and therefore enable particles to travel further south.

1. Introduction

The separation of the East Australian Current (EAC), the western boundary current flowing southward along the east coast of Australia, plays a dominant role in the flow pattern within the Tasman Sea. While transporting heat and biota from the Coral Sea to the Tasman Sea, the EAC separates into an eastward current at approximately 34°S known as the Tasman Front and a southward branch forming the EAC extension [e.g., *Godfrey et al.*, 1980; *Ridgway and Dunn*, 2003]. Volume transports of both pathways have been previously estimated at ∼9.7 Sv for the extension of the EAC [*Oliver and Holbrook*, 2014] and between -4 Sv and 18 Sv for the Tasman Front [*Sutton and Bowen*, 2014], although the highly variable nature of the EAC region makes accurate estimates difficult. Due to the ratio of eddy kinetic energy to mean kinetic enery of 500:1 in the EAC region compared to 10:1 of the global average, the EAC current system is highly variable and dynamic [e.g., *Mata et al.*, 2006; *Scharffenberg*, 2010].

The Tasman Front, which is the eastward flowing meander of the EAC, is a surface intensified flow that is confined to the upper 800m [*Sutton and Bowen*, 2014]. The front is shallower than the EAC, which itself extends to a depth below 2000m. *Sutton and Bowen* [2014], using a year-long deployment of current meters over a moored array deployed south of Norfolk Island, hypothesize that part of the deeper water of the EAC that does not flow along the Tasman Front, forms leakage past the south of Tasmania into the Indian ocean. Model studies show that this Tasman Leakage, fed by the extension of the EAC, is located in the upper 1000m of the ocean and its core is centered around 100m depth

[*Van Sebille et al.*, 2012]. Whether this water indeed originates from the deeper part of the EAC has not yet been investigated.

From previous studies, three main theories concerning the separation of the EAC can be distinguished. First, observations of the EAC region show that the separation of the EAC often takes plays near Sugarloaf Point at 32.4°S, where the coastline has a strong curvature [*Godfrey et al.*, 1980]. This suggests that the separation is topographically controlled. Indeed, *Marchesiello and Middleton* [2000], using a vorticity balance model study, find that a bend in the continental slope is the determinant factor to cause the EAC to separate in combination with the forcing from baroclinic Rossby waves pinching off eddies from the EAC. However, other studies argue that Rossby waves are not the main players in controlling the formation of the EAC eddies and that this variability is generated locally around the separation latitude [*Bowen et al*, 2005; *Mata et al.*, 2006].

In contrast, *Tilburg et al.* [2001] argue that bottom topography and coastline details have little effect on the separation latitude. Using numerical simulations whose complexity is systematically increased, they find that the inclusion of wind forcing results in the correct separation latitude, where gradients in the zonally integrated wind stress curl field determine the location. Analysis of sediment cores from the Coral Sea and the Tasman Sea show that during the last glacial the EAC separation took place between 23°S and 26° [*Bostock et al.*, 2006]. *Bostock et al.* [2006] mention the possibility that the shift is caused by a change in the wind stress curl field in the last glacial, but argue that this has not yet been proven and that the separation seems to be primarily controlled by SST gradients. Furthermore, *Oliver and Holbrook* [2014], using climate change simulations of the Tasman Sea circulation, show that the separation latitude may shift 100 km southwards from

1990 to 2060. *Oliver and Holbrook* [2014] argue that the linear Sverdrup theory can not explain the southward shift and that the mean location of the separation is governed by baroclinic, eddy-rich dynamics. Additionally, a shift in the separation latitude suggests that the dynamics of the separation latitude is not only topographically controlled.

Lastly, the separation of a western boundary current can also occur for reasons of vorticity dynamics, even in the absence of changes in the wind stress curl, bathymetry or a curvature of the coastline [*Kiss*, 2002]. Under no-slip boundary conditions the potential vorticity of the viscous sublayer of the western boundary current becomes larger than the potential vorticity of the interior. *Kiss* [2002] shows that the excess potential vorticity can only be dissipated by an outflow separating from the coast. This theory has not yet been investigated using oceanic general circulation models.

The different theories show the complexity of the western boundary current systems and the different mechanisms that affect their separation point. Modelling a realistic western boundary current separation is very sensitive to choices made for subgrid scale parameterizations and is sensitive to for example a proper representation of water mass properties, bathymetry and air sea fluxes. Despite the long history of research on modelling western boundary currents, there is not yet a single recipe that guarantees a correct separation of all western boundary currents in a global model [*Chassignet and Marshall*, 2008].

This paper is one of the first attempts to investigate the upstream control and the potential vorticity structure of the water masses separated at the bifurcation of the EAC separately from a Lagrangian perspective. Previous studies show that the Lagrangian approach is suitable in this region [e.g., *Van Sebille et al.*, 2012; *Cetina-Heredia et al.*, 2014]. An additional advantage of using a Lagrangian perspective is that, unlike an Eulerian approach, the direct connectivity between sources and sinks can be studied.

In this study, we use numerical Lagrangian float trajectories advected within a 1/4 degree global ocean sea-ice model, which allows us to make a distinction between water flowing eastward following the Tasman Front and water continuing southwards in eddies forming the EAC extension. This will give an idea of where and how the bifurcation of the EAC is controlled. We will investigate the upstream control of the fate of the water by studying the distribution of the particles upstream and downstream of the separation latitude. Furthermore, anomalies and changes in the in-situ potential vorticity structure for the two pathways upstream and around the separation latitude is studied to show what components of the potential vorticity equation are controlling the structure of the PV anomaly and how this relates to the bifurcation of the two pathways.

The next section presents a brief description of the ocean model used, the set-up of the Lagrangian experiment and how the distinction between the pathways is made. Additionally, the calculations made to analyse the potential vorticity of the pathways are discussed. Section 3 will provide a brief validation of the ocean model, followed by the analysis of the trajectories of interest in section 4, including an examination of the potential vorticity changes at the region of the EAC separation, followed by a general discussion and summary of our main results in section 5.

2. Data and Method

2.1. The ocean circulation model

To investigate the EAC separation we have used 5-day averages of the Geophysical Fluid Dynamics Laboratory (GFDL) Modular Ocean Model (MOM025), which is based on the ocean component of the GFDL CM2.4 and CM2.5 coupled climate models [*Farneti et al.*, 2010; *Delworth et al.*, 2012]. MOM025 is a global ocean-sea-ice model with 50 levels in the vertical (with a 10m resolution in the upper 100m up to a 200m resolution in the bottom layers) and a 1/4° eddy-permitting horizontal resolution with no-slip lateral boundary conditions, coupled to the GFDL Sea Ice Simulator dynamic/themodynamic sea-ice model. The atmospheric state is prescribed and converted to ocean surface fluxes by bulk formulae. There are no air-sea feedbacks and for the analysis a "normal year" atmospheric forcing is used constructed from version 2 of the Coordinated Ocean-ice Reference Experiments Normal Year Forcing (CORE-NYF) reanalysis data [*Griffies et al.*, 2009; *Large and Yeager*, 2009]. CORE-NYF consists of a climatological mean atmospheric state at 6 hour intervals for 1 year and includes synoptic variability. However, there is no interannual variability present in the forcing fields and all variability seen in the model output on time scales larger than a year can therefore only be caused by internal ocean processes, which are the main focus of this study. A run forced by Inter-Annual Forcing (CORE-IOF) version 2.0 is used for validation as well, to see to what extent atmospheric variability accounts for differences between the model run with normal year forcing and observations.

2.2. Particle tracking

The Lagrangian particles are released every 5 days for 10 years upstream of the EAC separation and advected forwards in time with a timestep of 1 hour within the 5-day averages of the 3D velocity field output of the ocean model, using the Connectivity Modeling System [CMS v1.1, *Paris et al.*, 2013]. No horizontal or vertical diffusivity is added to the particles, so the particle motion is purely advective. The particles are released at a zonal transect at 26°S between 154°E and 155.5°E within the top 1000m. Since particles flowing at depths deeper than 1000m are mainly recirculated in the Tasman Sea [*Ridgway and Dunn*, 2003], they are not considered as part of the two pathways of interest. Particles reaching the southern end of the Australian continent, between 42.5°S and 41.5°S and between 148°E and 150°E, are defined here to form the extension of the EAC. Particles flowing through a box north of New Zealand, between 31°S and 36°S and between 173.5°E and 175°E, are defined here as taking the Tasman Front pathway (figure 1). This way, a total of 1.4x10^5 particles that follow the Extension of the EAC and 1.1x10^5 particles that follow the Tasman Front are advected for up to 4 years, to make sure that the majority of the particles following the extension of the EAC had enough time to pass the southern tip of Tasmania [*Van Sebille et al.*, 2012].

2.3. Potential vorticity along the trajectories

The decomposition of the two pathways of interest allows us to investigate differences in anomalies in potential vorticity around and upstream of the separation latitude. Looking not only at anomalies in potential vorticity, but also at anomalies of relative vorticity and stratification will show which component is controling the structure of the PV anomaly and how this relates to the bifurcation of the two pathways. The same approach is used to look at changes in the potential vorticity terms along the trajectories to see if and where these terms are conserved.

For all particles, and for every 5 days along their trajectories, the in-situ potential vorticity (PV) at their longitude, latitude and depth is calculated using the vertical component of the Ertel PV

$$q = -\frac{f + \zeta}{\rho_{ref}} \frac{\partial \rho}{\partial z}, \tag{1}$$

where q is potential vorticity, f the planetary vorticity, ζ the relative vorticity, ρ_{ref} the reference density of 1035 kg/m^3 and ρ the in-situ density, where $\partial\rho/\partial z$ is a measure of stratification [e.g. *Dijkstra*, 2008]. First, q, ζ and $\partial\rho/\partial z$ are calculated from the velocity and density fields from the ocean model by central differencing. Then, the fields are linearly interpolated over a 0.1° lon x 0.1° lat x 10m depth grid and lastly, the obtained PV values are interpolated onto the location and time of the particles using a nearest-neighbors search.

The value of stratification is negative at all times, since the water columns in the ocean model used are statically stable everywhere. The planetary vorticity is negative in the southern hemisphere and is in most places larger in magnitude than the relative vorticity. The minus sign in equation 1 is chosen such that the potential vorticity will be negative in most locations in order to match other definitions of potential vorticity. If the Richardson number ($\mathrm{Ri} = N^2/|\partial\mathbf{u}_h/\partial z|^2$, where N^2 is the vertical buoyancy gradient and $\mathbf{u}_h$ the horizontal velocity) of the flow is large, so vertical shear and horizontal density gradients are small, q is conserved when following a water parcel in the absence of diabatic and frictional processes.

3. Validation of the Modular Ocean Model circulation

The ocean components of the next generation of climate models, which will form the bulk of CMIP6, will likely be eddy-permitting at a $1/4°$ – $1/3°$ horizontal resolution. This means that, even though a $1/4°$ model might not capture all dynamical aspects by under-estimating the eddy activity, it is still important to understand the physical mechanisms that are present in ocean models at this resolution. To validate the results of the model, a comparison is made between the model output and observed sea surface height (SSH) from the Archiving Validation and Interpretation of Satellite Oceanographic date (AVISO) by investigating the mean, the variability, the location of EAC separation and the volume transport. The AVISO product used provides SSH on a 0.25° by 0.25° Cartesian grid with a 7-day temporal resolution from 1992 to 2010.

3.1. Mean and Variability of the Sea Surface Height

The mean and the standard deviation of the sea surface height are calculated from the model and AVISO altimetry data (figure 2) over the entire length of the datasets (19 years for AVISO, 40 years for the model). The results from the model are not strongly dependent on the length of the dataset chosen to analyse, since interannual variability is low. The mean of the SSH is in good agreement with observations and the pathway of the EAC is clearly visible (figure 2a and 2b). However, the standard deviation, which is a measure for the variability or eddy activity, differs between the model and observations (figure 2c and 2d). The Tasman Front in the model seems to have a very narrow band of variability extending eastward at approximately 33°S, whereas in the satellite observations this pathway is not as clearly visible and seems to be more broad. Furthermore, the variability in the model shows only half the magnitude of the variability seen in AVISO.

Van Sebille et al. [2012] studied the same region using the Ocean Forecast for the Earth Simulator (OFES), which is based on an older version of the Modular Ocean Model (MOM3), but has a 1/10° horizontal resolution. They find a good agreement in SSH variability between AVISO and their model output, suggesting that the lower resolution of MOM025 leads to reduced SSH variability. Furthermore, ∼30% of the missing variability in the region of the EAC separation can be explained by interannual atmospheric variability, comparing the model run with 'Normal-Year' forcing to the model run with

'Inter-Annual' forcing (not shown). Therefore, it is likely that the underestimation in variability is mainly due to the relatively low horizontal resolution in the ocean model, with a smaller effect of the missing atmospheric interannual variability in the forcing.

3.2. Separation latitude of the EAC

In order to validate the model further, the time series of the EAC separation latitude is used to compare the location and variability of separation between the model and AVISO. The method of estimating the latitude at which the EAC veers eastward is based on a modified version of the method described by *Cetina-Heredia et al.* [2014], where SSH contours are used to find the veering point of the main current. First, the core of the EAC is found upstream of the separation by selecting the maximum southward geostrophic surface velocity at a 28°S transect. Second, the SSH isoline coinciding with the location of the maximum velocity is followed. Third, the location at which the isoline turns more than 30 degrees eastward of south is recorded as the separation latitude. This method has been shown to be appropriately sensitive to both eddy detachment and reattachment, which highly influence the location of separation [*Cetina-Heredia et al.*, 2014]. The chosen threshold of 30 degrees might result in values of the separation latitude that are slightly further to the south than in-situ observations indicate. By the time the SSH contour has turned 30 degrees, its actual separation from the coast has already taken place further north. However, since we use the same method for the model data and the observation from satellite altimetry, this is still a good method to validate the models representation of the separation.

The temporal average of the separation latitude over the years of data available shows a clear dependance on the seasonal cycle (figure 3a). The standard deviation in the separation latitude of the model is 0.5° to 1° (figure 3c), while the standard deviations in the observations is much larger (figure 3b), so this cycle will not be very clear in most years and only shows up in the mean. In both the model and the observations the most northern separation latitude is reached in July, whereas the most southern latitudes are reached between December and April. This is in agreement with the in-situ observed enhanced southward flow of the EAC in summer [*Ridgway and Godfrey*, 1997]. Furthermore, the time series show some skewness, with a steeper slope of the EAC separation retraction northward compared to the progression of the separation southwards. This can be explained by the observed higher eddy kinetic energy in late summer and autumn in this region, implying more eddy shedding events [*Qiu et al.*, 2004; *Cetina et al.*,2014] (figure 3c).

The cumulative probability of the time series obtained shows the underlying distribution of the separation latitude (figure 3b). Per degree of latitude at which the maximum southward geostrophic velocity is selected, the median of the probability can shift southwards or northwards by 0.3-0.4° latitude. However, the shape of the function stays the same. Therefore, it is possible to use this method to compare the underlying distribution of both datasets.

From this, we can conclude that the median of the separation latitude in the model agrees very well with the observations. The distribution of the modeled separation latitude is however much narrower, consistent with the model's underestimation of SSH variability. This, again, can be explained by the relatively low horizontal resolution in the ocean model and the effect of the missing atmospheric variability in the forcing. The difference of the recorded separation latitude between the model and the AVISO data is slightly larger at the southern end of the distribution than at the northern end of the distribution. It is likely that this skewness is caused by the observed trend in the EAC separation latitude, where the current is found to separate more often at the southernmost latitudes in more recent years [*Cetina-Heredia et al.*, 2014].

3.3. Volume transport in the Tasman Sea

The volume transport in the Tasman Sea is calculated for different sections by multiplying the normal velocity component with the grid area and integrating over the upper 2000m of the water column. The transport is compared to estimates derived from the mean dynamic topography relative to 2000m from CSIRO Atlas of Regional Seas (CARS) climatology [*Oliver and Holbrook*, 2014; *Ridgway et al.*, 2002; *Dunn and Ridgway*, 2002; *Condi and Dunn*, 2006] and estimates given by *Ridgway and Godfrey* [1994] based on observations of 6000 hydrological stations. The different segments are indicated by letters chosen to match *Oliver and Holbrook* [2014] (figure 4).

At the northern boundary of the Tasman Sea, the inflow from the EAC (EF, figure 4) and the flow northward across 28°S (DE) in the model are both lower than the volume transport estimated from observations, indicating that the EAC strength is weaker in the model than in observations. The transport across the meridional section at 173°E (DG) is however overestimated. Similar to the results from the standard deviation of the SSH and the findings of *Oliver and Holbrook* [2014] this suggests that the model predicts a more focused eastward flow along the Tasman Front than observations do. At the southern boundary of the domain, the model estimates for the narrow flow along Tasmania from the EAC extension (AB) are similar to the observations. The northward transport is slightly overestimated (BC).

The net transport out of the domain bounded by A-F (figure 4) of the ocean model is 0.6 Sv compared to -0.8 Sv estimated from CARS and 2.2 Sv estimated by *Ridgway and Godfrey* [1994]. The imbalance in the model can be explained by leakage through the Cook and Bass straits and the transport taking place at depths below 2000m. The imbalance for the observations are larger and of opposite sign, indicating that the observed values are uncertain as well, which is partly caused by the highly variable transport in this region.

The Lagrangian particles advected in the ocean model are used to provide a second method to estimate transport. Every particle is tagged with its transport at the time of release by multiplying the southward velocity with the area (0.25° lon x 10m thickness). From this an estimate can be made for the proportion of water that originates from the EAC and follows the Tasman Front or follows the extension of the EAC. The results show that a large part (∼40%) of the transport from the EAC is following the Tasman Front pathway and only ∼14% of the total transport is following the extension of the EAC. The remainder of the transport in the EAC is carried by particles that recirculate within the Tasman Sea and do not reach Tasmania or New Zealand (figure 1). This is in agreement with previous estimates that show a 1:3 ratio between transport in the extension of the EAC and transport in the Tasman Front [*Hill et al.*, 2011].

We conclude that, although the model does not reproduce all features of the East Australian Current region as seen in observations, it shows sufficient skill to assess the two pathways resulting from the EAC separation from the coast.

4. Results

4.1. Upstream control by particle distribution

The depth profile of the particle density distribution upstream of the separation latitude at 28°S is shown in figure 5 for particles traveling southwards as part of the EAC extension and for particles traveling eastwards along the Tasman Front. A clear distinction in the distribution of the particles with depth between the two pathways can be observed, but the zonal distribution is very similar. 83% of the particles following the extension of the EAC originate from the deeper part of the EAC flow between a depth of 640m and 1000m. The particles that form part of the Tasman Front, however, originate from the upper part of the EAC, where 72% originates from the layer between the surface and 640m depth. Shifting the chosen transect southwards or northwards upstream of the separation location does not change this distribution (not shown). There are no particles in this simulation that originate from a depth deeper than 700m ending up north of New Zealand while following the Tasman Front, in agreement with the observed values by *Sutton and Bowen* [2014]. This indicates that whether a particle follows the Tasman Front or the EAC extension (the 'fate' of a particle) is to some extent already determined before the EAC bifurcates.

The distribution in the water column does not change significantly following the particle trajectories. The change in depth from before the bifurcation, at 27°S, to after the bifurcation, at 40°S and 160°E for the extension of the EAC and the Tasman Front particles respectively, is shown in figure 6. The particles originating from 200m-600m depth, that follow the extension of the EAC (figure 6a), seem to be advected upward in the water column by up to 200m. Below 600m the particles do not seem to change their depth significantly. The particles that follow the Tasman front show a mean shift upwards of only 50m (figure 6b) and their distribution in the water column has a smaller extent than the particles that follow the extension of the EAC.

This behavior can be explained by the outcropping of time-mean isopycnals. We note the presence of isopycnal outcropping in the top 300m depth from 27°S to 40°S (dotted line figure 6a). From 300m to 700m depth, the isopycnals move strongly upwards in the water column, and below 700m their depth does not change. The behavior of the isopycnals in this region is mainly explained by the strong gradient in temperature over the transects chosen. Comparing the depth of the isopycnals between the transects at 27°S and 160°E along the Tasman Front, the isopycnals are slightly pushed up (dotted line figure 6b), which is explained by the fact that the transect at 160°E lies poleward of 27°S around 34°S where the mean density is higher.

The results indicate that particles tend to adiabatically follow isopycnals. It seems that particles following the extension of the EAC only partly follow isopycnals, as seen in the differences between the curve of the particles depth change and the curve of the depth change of the isopycnals (figure 6a). However, a large part of these particles might be trapped in warm-core anticyclonic eddies and therefore experience a lower density than the mean flow around them at the transect at 40°S. This could mean that these particles do follow isopycnals, but experience a smaller upward advection than the mean density surfaces show.

To investigate whether the displacement of the particles is due to vertical movement of isopycnals or due to mixing across isopycnals, the change of the particle's density between the transects (27°S to 40°S and 27°S to 160°E) is calculated (figure 7). Respectively 80%

and 67% of the particles density change is within a $\pm$ 0.2 kg/m^3 range from the identity line for particles following the extension of the EAC and particles following the Tasman Front. From this, it is clear that particles tend to follow isopycnals. Therefore, the discrepancy seen in figure 6a between the curve of the particles change in depth from 27°S to 40°S and the curve of the change of depth of the isopycnals can indeed be explained by the fact that most of the particles in the upper 600m are travelling southwards within anticyclonic eddies, and show less advection upwards than the mean isopycnal field.

4.2. Control by eddy activity

The number of particles crossing the transect at 28°S varies with time. For the subset of particles that follow the EAC extension the largest fraction crosses the transect in September (14.5 %, figure 8a) and the smallest fraction crosses the transect in May (3.8 %). The percentages shown are normalised for each pathway individually. Although there is some variability seen in the subset of the particles that follow the Tasman Front, it does not show a seasonal dependance. Therefore, less water flowing into the extension of the EAC does not necessarily lead to more water following the Tasman Front and vice versa.

Depending on which latitude is chosen for the transect, the peak of the maximum fraction of particles crossing that transect shifts to later or earlier months if the transect shifts southwards or northwards respectively. This shift can be explained by the time it takes particles to cover the distance from the transect at 28°S to the separation latitude. The transit time from the transect at 28°S to the mean separation latitude of 33°S is shown, in a cumulative sense, in figure 8b for the particles that cross 28°S in September. Half of the particles arrive at 33°S within 4 months, but the distribution ranges from transit times of a miminimum of 22 days to transit times of more than a year. This suggests that a large fraction of particles is trapped in eddies north of the mean separation latitude of 33°S. Furthermore, investigation of the particles trajectories reveals that some particles take a long detour away from the coast and the EAC before reaching 33°S, which are not shown in figure 1. With a delay of 4 months, the arrival time at the separation region of the maximum number of particles following the EAC extension is January.

The strong seasonal variability seen in the number of particles following the extension of the EAC is likely related to the strong seasonal variability observed in the EAC separation latitude (figure 3a) and the eddy activity (figure 3c). In western boundary current regions the standard deviation in sea level height is mostly caused by mesoscale eddy variability [*Zlotnicki et al.*, 1989; *Thompson and Demirov*, 2006] and can therefore be used as an indicator for eddy activity. To obtain the time series of the SSH standard deviation in the ocean model, a 55-day running mean is used and the result is averaged over the area between 20°S and 45°S and between 150°E and 160°E.

The eddy activity and the variability seen in the separation latitude are highly correlated (figure 3c). As discussed in section 3.2, this can be explained by the eddy shedding process, where higher eddy activity implies more eddy shedding and therefore larger variability in the separation latitude. The variability is high from January through to June, while the separation latitude moves equatorward from its most southern excursion (figure 3a). The maximum variability seems to be reached in June, which is a few weeks before the most northern separation latitude is reached (figure 3). Then, the variability quickly drops down to a minimum in October and starts slowly increasing from October onwards. Combining this result with the transit time from 28°S to 33°S (figure 8b), it seems that the number of particles ending up in the extension of the EAC is dependent on the eddy activity and where the separation takes place. The results suggest that the largest transport across the separation latitude takes place around January, when the eddy activity is high and the EAC separates at the southern end of its range.

4.3. Control by potential vorticity

The future pathway of the particles seems to be mostly controlled inside the EAC by the depth of the particles upstream of the separation latitude (section 4.1). However, as seen in figure 5, there is an overlapping region between the surface and a depth of approximately 600m where the particles can either follow the extension of the EAC or the Tasman Front. This section will focus on the evolution of vorticity for both particle pathways in the overlapping region at about 400m depth, where the number of particles of both pathways is optimum.

To investigate what determines whether a particle in the overlapping region veers eastward into the Tasman Front or continues southward, anomalies of potential vorticity, stratification and relative vorticity are calculated for both pathways (figure 9). Particles are selected when traveling through one of the 0.1° lon x 0.1° lat grid boxes in a thin depth layer between 350m and 450m depth, where the particles of both pathways are evenly distributed and the density does not change significantly with depth. The values shown are averages over 100 randomly selected particles at that grid point, to be sure that the results are not biased by the number of particles present. All locations containing less than 100 particles are not shown.

The resulting anomalies in the potential vorticity terms are 5-10 times smaller than the values for the mean potential vorticity and $\partial\rho/\partial z$ and roughly 2 times smaller than the values of the mean relative vorticity. From 33°S to 38°S, particles located close to the coastline have a standard deviation of similar magnitude compared to the anomaly itself at that location. This indicates that there is a high variabiliy of vorticity in this region and therefore the anomaly close to the coast south of 33°S should be interpreted carefully.

There is a clear difference between the two pathways in the anomalies for all the vorticity terms upstream of and around the separation latitude. The potential vorticity anomaly is strongly positive at the eastern side of the particle trajectories following the extension of the EAC (figure 9a). In the same region, the particles following the Tasman Front show a negative anomaly in potential vorticity (figure 9b). For both pathways, this region falls outside the regions with a large spread in potential vorticity, and the difference observed between the anomalies in q of particles following the extension of the EAC and particles following the Tasman Front is therefore robust. These patterns are mainly caused by the anomalies seen in the stratification (figures 9c and 9d), which indicates that layer thickness variations are dominating the structure of potential vorticity.

Between 30°S and 32°, $\partial\rho/\partial z$ shows a positive anomaly, indicating a decrease in stratification from the mean (figure 9c). To explain why the particles experience a reduction in the stratification of the fluid, it is important to know where the pycnocline is located and how eddies influence the density profile in this region. In the mean state of the density profile the maximum in density changes, the pycnocline, is located at 400m depth north of 32°S (not shown). From 32°S to 34°S a sharp decrease in depth of the pycnocline is observed, coinciding with the outcropping of warm Coral Sea water. Since the depth of our layer chosen is located at the pycnocline depth in the northern region of our domain, upward or downward shifting of the pycnocline would both cause a reduction in stratification. The same region shows a positive anomaly in relative vorticity (figure 9e), indicating more anticyclonic behavior compared to the mean. Anticyclonic eddies have the tendency to push isopycnals, and therefore the pycnocline, down. Apparently, particles flowing along the EAC extension experience more anticyclonic behavior, which causes a reduction in the stratification and potential vorticity around 32°S.

The particles that follow the Tasman Front show a negative anomaly in $\partial\rho/\partial z$, indicating an increase in stratification with respect to the mean state. The negative signature is even stronger farther south. It is possible that this behavior is not caused by vertical changes in the pycnocline, as for the particles following the EAC extension, but by a horizontal shift of the outcropping region of the pycnocline. Shifting this region to the south would bring the more stratified water of the pycnocline to a region of less stratified water at the depth of 400m, explaining the observed anomaly in stratification. This is an indication that particles following the Tasman Front are controlled by the strong horizontal gradient in density seen in the upper 400m around 33°S, caused by the outcropping of isopycnals. Particles following the Tasman Front can only reach higher latitudes when this barrier is pushed southwards.

The anomaly in relative vorticity for particles following the Tasman Front shows a positive anomaly close to the coast following the southern boundary of the particles trajectories, but a slightly negative anomaly away from the coastline (figure 9f). Interestingly, the mean state of relative vorticity shows a similar pattern with negative (cyclonic) and positive (anticyclonic) regions (not shown). The cyclonic regions coincide with the regions where we see a positive anomaly in relative vorticity and the anticyclonic regions coincide with the regions where we see a negative anomaly in relative vorticity. This indicates that particles following the Tasman Front experience a reduction in both anticyclonic and cyclonic behavior compared to the mean. The reduction can be caused by either less eddy activity or by a weakening of the flow.

Combining the results of the anomalies seen in the vorticity terms it seems that to cross the barrier of strong horizontal density gradients, anticyclonic eddies play a crucial role in pushing isopycnals down and transporting particles southwards.

We have seen that layer thickness variations are dominating the structure of potential vorticity. However, this does not necessarily imply that potential vorticity changes along particle trajectories are dominated by stratification changes. Since particles to first order follow contours of constant isopycnal spacing, the contribution to Lagrangian PV change from stratification is reduced. Therefore, we also compute the material derivative of potential vorticity, stratification and relative vorticity along the trajectory of the particles and visualize these in the same way as the anomalies of these terms (figure 10). The results show the change along a trajectory over 5 days. The standard error of the mean is at least one order of magnitude smaller than the calculated values (not shown), indicating that the means shown are statistically different from zero.

The results for the particles following the extension of the EAC and the results for particles following the Tasman Front show a similar pattern. It is clear that potential vorticity is relatively well conserved on the offshore side of the domain. However, close to the coast changes in potential vorticity are sigificant where an $O(1)$ change of PV can take place within 50 days. Since the model has no-slip boundary conditions it is possible that friction causes the PV conservation to break down in this region.

North of 31°S the potential vorticity is decreasing downstream at the onshore side of the current and increasing downstream at the offshore side (figure 10a and b). Comparing this region to the patterns seen for the temporal change in $\partial\rho/\partial z$ (figure 10c and d) and relative vorticity (figure 10e and f), the changes in PV are due to changes in relative vorticity, rather than changes in stratification. The relative vorticity shows a decrease in ζ at the cyclonic side and an increase in ζ at the anticyclonic side, implying that both cyclonic and anticyclonic behavior is increasing downstream. This is in agreement with previous studies on western boundary current dynamics [*Kiss*, 2010].

The pattern seen in the Lagrangian changes in relative vorticity at the offshore side of the domain (figure 10f), can be explained by the fact that potential vorticity is mostly conserved in this region. Since $\partial\rho/\partial z$ does not show any significant changes in this region as well, poleward movement requires an increase in relative vorticity and equatorward movement a decrease in relative vorticity to conserve PV (see equation 1), which agrees with the path the particles take and the changes in relative vorticity seen in figure 10f.

South of 32°S the pattern of the Lagrangian changes in potential vorticity is reversed, with increasing values of potential vorticity along the coastline and decreasing values offshore (figure 10a). This pattern can be explained by the changes seen in the $\partial\rho/\partial z$ term (figure 10c). Particles feel a stretching of isopycnals when they travel close to the coast along their trajectory and a squeezing offshore. The signal follows the coastline closely and the width of the region where the changes take place is about 200 km. Since southward traveling eddies take exactly this route they might induce the pattern seen here. Anticyclonic eddy motion is southward near the coast and northwards offshore. The cross-shore component cancels out in the mean as an eddy moves south. However, the alongshore component can cause an increase (decrease) in potential vorticity at the onshore (offshore) side of the eddy, due to a decrease (increase) in the stratification magnitude seen in figure 10c.

5. Discussion

In this paper we have used Lagrangian particles advected in the Modular Ocean Model to investigate where and how the fate of the particles following the EAC extension and the Tasman Front is controlled. We have seen that the pathway of the particles downstream of the separation is to some extent already determined by the particles distribution within the EAC current upstream of the separation latitude, where the surface waters follow the Tasman Front and the deeper waters (till 1000m depth) follow the extension of the EAC. In the region where the two water masses overlap, at 400m depth, the fate of the water seems to depend on the presence of anticyclonic eddies that push the isopycnals down enabling particles to travel further south.

The fact that the Tasman Front pathway is fed by water from the top 600m of the EAC agrees well with the observations done by *Sutton and Bowen* [2014]. Furthermore, this study shows that the water located deeper in the EAC is indeed travelling southwards as hypothesized by *Sutton and Bowen* [2014]. We have seen that the particles travelling southwards between 600m and 1000m depth do not really change their depth in the water column, whereas particles travelling in the upper 600m are slightly advected upwards. Studying the change in density of the particles between 27°S and 40°S shows that the vertical displacement is due to the adiabatic behavior of the particles. Particles following the Tasman Front keep their density constant by veering eastward instead of displacing vertically.

The results of this study show that the structure of the isopycnals is dominant in splitting the two pathways. Particles travelling below 600m do not experience a strong vertical change in the isopycnal which they are following and are therefore able to continue their journey southwards along the eastern boundary of Australia. Particles in the upper 600m however experience a strong gradient in the horizontal density field around the separation latitude, due to the outcropping of isopycnals, and most of the particles are forced to continue their journey eastward.

Vertical and horizontal shifts in the pycnocline could explain the anomalies seen in the stratification and potential vorticity. From the results, it is also clear that layer thickness variations are dominating the structure of potential vorticity in this region. The vertical downward shift of the pycnocline is explained by the increased anticyclonic behavior around the separation latitude in figure 9e. This could mean that anticyclonic eddies are essential for transporting water across the horizontal gradient in density in the top layer. The negative anomaly in the stratification for particles following the Tasman Front could be explained by the southward movement of the vertical slope of the pycnocline. The movement of the front is related to the separation latitude of the EAC and since time series of the separation latitude show a clear seasonal cycle, one would expect a seasonal signal in the number of particles moving eastwards as well. However, there is no clear seasonal signal seen in the number of particles following the Tasman Front (figure 8a) and further investigation is necessary to see what is causing the anomaly in stratification.

The fact that anticyclonic eddies play a crucial role in the transport southwards in the upper layer connects well to the results seen in the seasonal dependence of the transport southwards (figure 8a) in relation to the seasonal pattern seen in the eddy activity (figure 3c). *Cetina-Heredia et al.* [2014] have looked at the amount of southward transport that takes place inside eddies and estimate that only 15.8 $\pm$ 18.3% of the transport takes place within eddies. However, this is calculated with respect to the total transport southwards, and not with respect to the transport taking place in the upper 600m. The transport southwards originating from the upper layer of the EAC current might show a larger percentage of water being transported inside eddies as the eddies are surface-intensified.

This paper is one of the first attempts to investigate the conservation of potential vorticity from a Lagrangian perpective in a general circulation ocean model. North of the separation latitude, an increase in cyclonic and anticyclonic behavior is observed downstream, causing the potential vorticity to decrease on the onshore, cyclonic, side of the current and increase on the offshore, anticyclonic, side. This in good agreement with the results found by *Kiss* [2010] that changes in PV are due to changes in relative vorticity rather than changes in stratification. On the cyclonic side, the potential vorticity becomes far more negative than the potential vorticity in the interior at the same latitude. This supports the idea that the 'excess' negative vorticity has to be lost to connect the fluid to the interior [*Kiss*, 2010]. In figure 10b for particles following the Tasman Front, a small positive region of the Lagrangian change of potential vorticity at 153.5°E and 33°S is observed, indicating the loss of negative vorticity which could be caused by the sudden decrease in cyclonic behavior in this region seen in figure 10f.

In this study, only the vertical component of the Ertel potential vorticity equation is considered. However, since we have seen that a sharp vertical slope in the pycnocline is observed at the separation latitude, the horizontal component (the baroclinic term) of the Ertel potential vorticity equation (given by $\boldsymbol{\omega}_h \cdot \boldsymbol{\nabla}_h(-\rho/\rho_0)$, where $\boldsymbol{\omega}_h$ is the horizontal component of the absolute vorticity $\boldsymbol{\omega} = f\hat{\boldsymbol{k}} + \boldsymbol{\nabla} \times \boldsymbol{u}$) might not be negligible in this region [*Holmes et al.*, 2014]. Indeed, *Godfrey et al.* [1980] find low Richardson numbers at the separation latitude indicating that horizontal density gradients and shear might be of importance. Consequently, the regions where we see non-conservation of PV in figure 10 could still be conserving the full potential vorticity when including the baroclinic term.

To asses whether friction, diabatic processes or the horizontal component of the Ertel PV are causing the potential vorticity to change along a particles trajectory, the vorticity balance has to be investigated. For this, an online assessment of the different potential vorticity terms is necessary to ensure a closing balance and the results would benefit from a higher temporal and horizontal resolution of the ocean model. A higher horizontal resolution would also result in a more realistic representation of the eddy field and a higher temporal and horizontal resolution would decrease the errors made when interpolating the potential vorticity fields to the particle location and moment in time.

Acknowledgments. This project was supported by the Australian Research Council via grant DE130101336. Sea surface height from the Archiving Validation and Interpretation of Satellite Oceanographic (AVISO) data was obtained from http://www.aviso.oceanobs.com/duacs.

References

Bostock, H.C., B.N. Opdyke, M.K. Gagan, A.E. Kiss, and L.K. Fifield (2006), Glacial/interglacial changes in the East Australian current, *Climate Dynamics*, *26*, 645–659.

Bowen, M., J.L. Wilkin, and W.J. Emery (2005), Variability and forcing of the East Australian Current , *J. Geophys. Res.*, *110*, doi:10.1029/2004JC002533.

Cetina-Heredia, P., E. van Sebille, and M.A. Coleman (2014), Long-term trends in the East Australian Current separation latitude and eddy driven transport, *J. Geophys. Res. Oceans*, *119*, doi:10.1002/2014JC010071.

Chassignet, E.P., and D.P. Marshall (2008), Gulf stream separation in numerical ocean models, *Ocean modeling in an eddying regime*, 39–61

Condie, S.A., and J.R. Dunn (2006), Seasonal characteristics of the surface mixed layer in the Australasian region: Implications for primary production regimes and biogeography, *Mar. Freshwater Res.*, *57*(6), 569–590

Delworth, T., A. Rosati, W. Anderson, A. Adcroft, V. Balaji, R. Benson, K. Dixon, S. Griffies, H.C. Lee, R. Pacanowski, G. Vecchi, A. Wittenberg, F. Zeng, R. Zhang (2012), Simulated climate and climate change in the GFDL CM2.5 high-resolution coupled climate model, *J. Climate*, *25*, 2755–2781.

Dijkstra, H.A (2008), Dynamical Oceanography, *Springer-Verlag Berlin Heidelberg.*

Dunn, J.R., and K.R. Ridgway (2002), Mapping ocean properties in regions of complex topography, *Deep Sea Res., Part I*, *49*(3), 591–604.

Farneti, R., T. Delworth, A. Rosati, S. Griffies, F. Zeng (2010), The role of mesoscale eddies in the rectification of the Southern Ocean response to climate change, *J. Phys.*

Oceanogr., *40*, 1539–1557.

Godfrey, J.S., G.R. Cresswell, T.J. Golding, and A.F. Pearce (1980), The separation of the East Australian Current, *J. Phys. Oceanogr.*, *10*, 430–439.

Godfrey, J.S., G.R. Cresswell, and F.M. Boland (1980), Observations of Low Richardson Numbers and Undercurrents near a Front in the East Australian Current, *J. Phys. Oceanogr.*, *10*, 301–307.

Griffies, S., A. Biastoch, C. Boning, F. Bryan, G. Danabasoglu, E. Chassignet, M. England, R. Gerdes, H. Haak, R. Hallberg, W. Hazeleger, J. Jungclaus, W. Large, G. Madec, A. Pirani, B. Samuels, M. Scheinert, A.S. Gupta, C. Severijns, H. Simmons, A.M. Treguier, M. Winton, S. Yeager, J. Yin (2009), Coordinated Oceanice Reference Experiments (COREs), *Ocean Modelling*, *26*, 1–46.

Griffies, S.M. (2012), Elements of the Modular Ocean Model (MOM), *GFDL Ocean Group Technical Report No.7*, 620 + xiii pages [available online at http://www.mom-ocean.org/web/docs].

Hill, K.L., S.R. Rintoul, K.R. Ridgway, and P.R. Oke (2011), Decadal changes in the South Pacific western boundary current system revealed in observations and ocean state estimates, *J. Geophys. Res.*, *116*, C01009, doi:10.1029/2009/JC005926.

Hobday, A.J. and K. Hartmann (2006), Near real-time spatial management based on habitat predictions for a longline bycatch species, *Fisheries Management and Ecology*, *13*, 365–380.

Holmes, R.M., L.N. Thomas, L. Thompson, and D. Darr (2014), Potential Vorticity Dynamics of Tropical Instability Vortices, *J. Phys. Oceanogr.*, *44*(3), 995–1011.

Kiss, A.E. (2002), Potential vorticity “crises”, adverse pressure gradients, and western boundary current separation,*Journal of Marine Research*, *60*, 779–803

Kiss, A.E. (2010), Dynamics of separating western boundary currents in ocean models,*IOP Conf. Series: Earth and Environmental Science*, *11*, doi:10.1088/1755-1315/11/1/012034

Large, W., S. Yeager (2009), The global climatology of an interannually varying air–sea flux data set, *Clim. Dyn.*, *33*, 341–364.

Marchesiello, P., and J.H. Middleton (2000), Modeling the East Australian Current in the Western Tasman Sea, *J. Phys. Oceanogr.*, *30*, 2956–2971.

Mata, M.M., S.E. Wijffels, J.A. Church, M. Tomczak (2006), Eddy shedding and energy conversions in the East Australian Current, *J. Geophys.Res. Oceans*, *111*, C09034.

Oliver, E.C.J., and N.J. Holbrook (2014), Extending our understanding of South Pacific gyre “spin up”: Modeling the East Australian Current in a future climate, *J. Geophys. Res. Oceans*, *119*, 2788–2805.

Paris, C.B., J. Helgers, E. van Sebille and A. Srinivasan (2013), The Connectivity Modelling System: A probabilistic tool for the multi-scale tracking of biotic and abiotic variability in the ocean, *Environ. Modell. Soft.*, *42*, 47–54.

Qiu, B., and S. Chen (2003), Seasonal modulations in the eddy field of the south pacific ocean, *J. Phys. Oceanogr.*, *34*(7), 1515–1527

Ridgway, K.R., and J.S. Godfrey (1994), Mass and heat budgets in the East Australian Current System: a direct approach, *J. Geophys. Res.*, *99*(C2), 3231–3248.

Ridgway, K.R., and J.S. Godfrey (1997), Seasonal cycle of the East Australian Current, *J. Geophys. Res.*, *102*(C10), 22,921–22,936.

Ridgway, K.R., J.R. Dunn, and J. Wilkin (2002), Ocean interpolation by four-dimensional weighted least squares-application to the waters around Australasia, *J. Atmos. Oceanic. Technol.*, *19*(9), 1357–1375.

Ridgway, K.R., and J.R. Dunn (2003), Mesoscale structure of the East Australian Current System and its relationship with topography, *Prog. Oceanogr.*, *56*, 189–122.

Roughan, M., P.R. Oke, and J.H. Middleton (2003), A modeling study of the climatological current field and the trajectories of upwelled particles in the East Australian Current, *J. Phys. Oceanogr.*, *33*(12), 2551–2564.

Schaeffer, A., M. Roughan, and B.D. Morris (2013), Cross-Shelf Dynamics in a Western Boundary Current Regime: : Implications for upwelling, *J. Phys. Oceanogr.*, *43*(5), 1042–1059.

Scharffenberg M.G., and D. Stammer (2010), Seasonal variations of the large-scale geostrophic flow field and eddy kinetic energy inferred from the TOPEX/poseidon and Jason-1 tandem mission data, *J. Geophys. Res.*, *115*, C02008, doi:10.1029/2008JC005242

Sutton, P.J.H., and M. Bowen (2014), Flows in the Tasman Front south of Norfolk Island, *J. Geophys. Res. Oceans*, *119*, 3041–3053.

Tilburg, C.E., H.E. Hulburt, J.J. O'Brien, and J.F. Shriver (2001), The dynamics of the East Australian Current System: The Tasman Front, the East Auckland Current, and the East Cape Current, *J. Phys. Oceanogr.*, *31*(10), 2917–2943.

Thompson, K.R., and E. Demirov (2006), Skewness of sea level variability of the world's oceans, *J. Geophys. Res.*, *111*, C05005, doi:10.1029/2004JC002839.

Van Sebille, E., M.H. England, J.D. Zika and B.M. Sloyan (2012), Tasman leakage in a fine-resolution ocean model, *Geophys. Res. Lett.*, *39*(6).

Zlotnicki, V., L.L. Fu, and W. Pratzert (1989), Seasonal variability in global sea level observed with Geosat altimetry, *J. Geophys. Res.*, *94*(C12), 17.959–17.969.

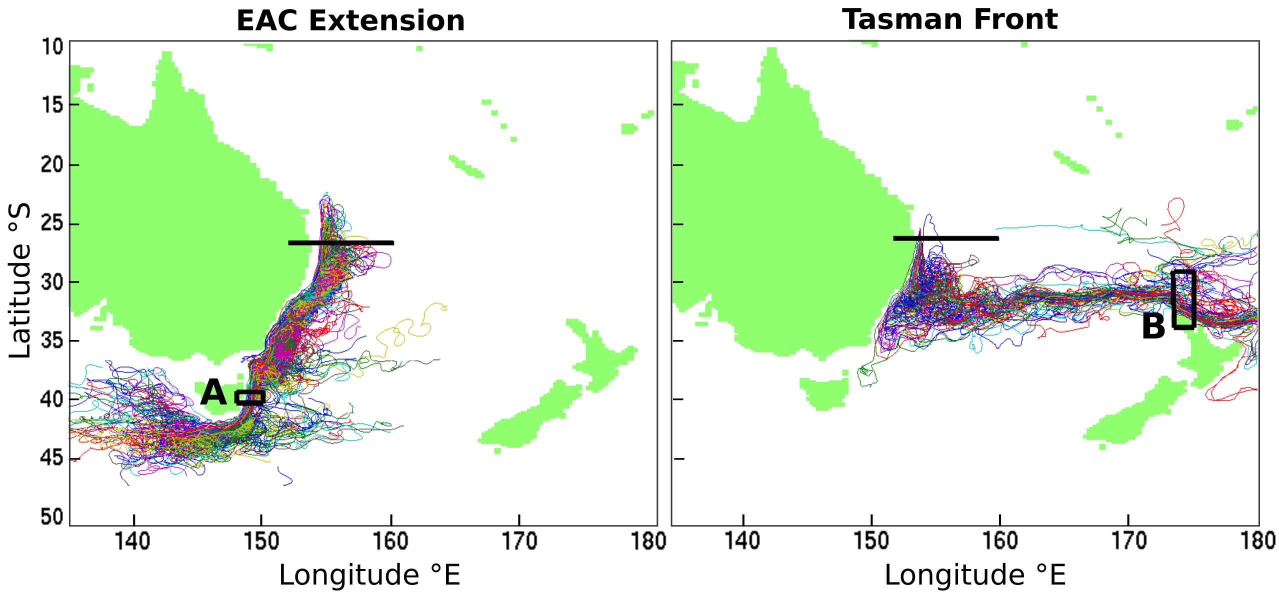

Figure 1. Subset of 80 particles, respectivily, advected in the ocean model following the pathway of the extension of the EAC (left) and the pathway of the Tasman Front (right) following their release at 27°S. Particles traveling through box A (41.5°S – 42.5°S and 148°E – 150°E) are selected to form the extension of the EAC. Particles traveling through box B (31°S – 36°S and 173.5°E – 175°E) form the pathway of the Tasman Front. The black line shows the transect at 28°S which is located upstream of the separation latitude. Coloring is random.

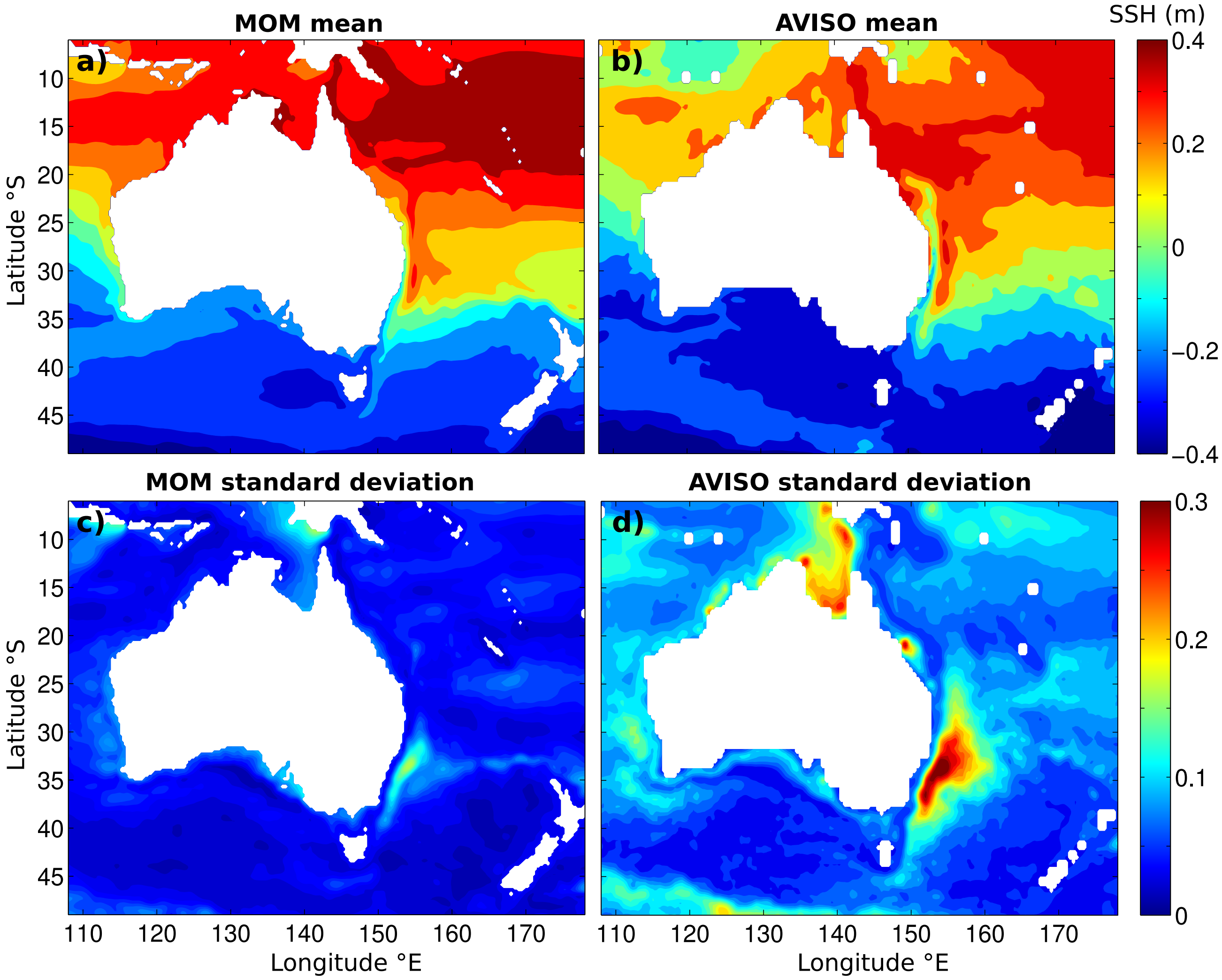

Figure 2. Mean and standard deviation of the Sea Surface Height (SSH) for the ocean model output (a,c) and for observation from AVISO satellite altimetry (b,d). The variability in SSH is strongly underestimated in the 1/4° MOM025 model output with normal year forcing. The model output with interannual atmospheric forcing accounts for 30% of the missing variability.

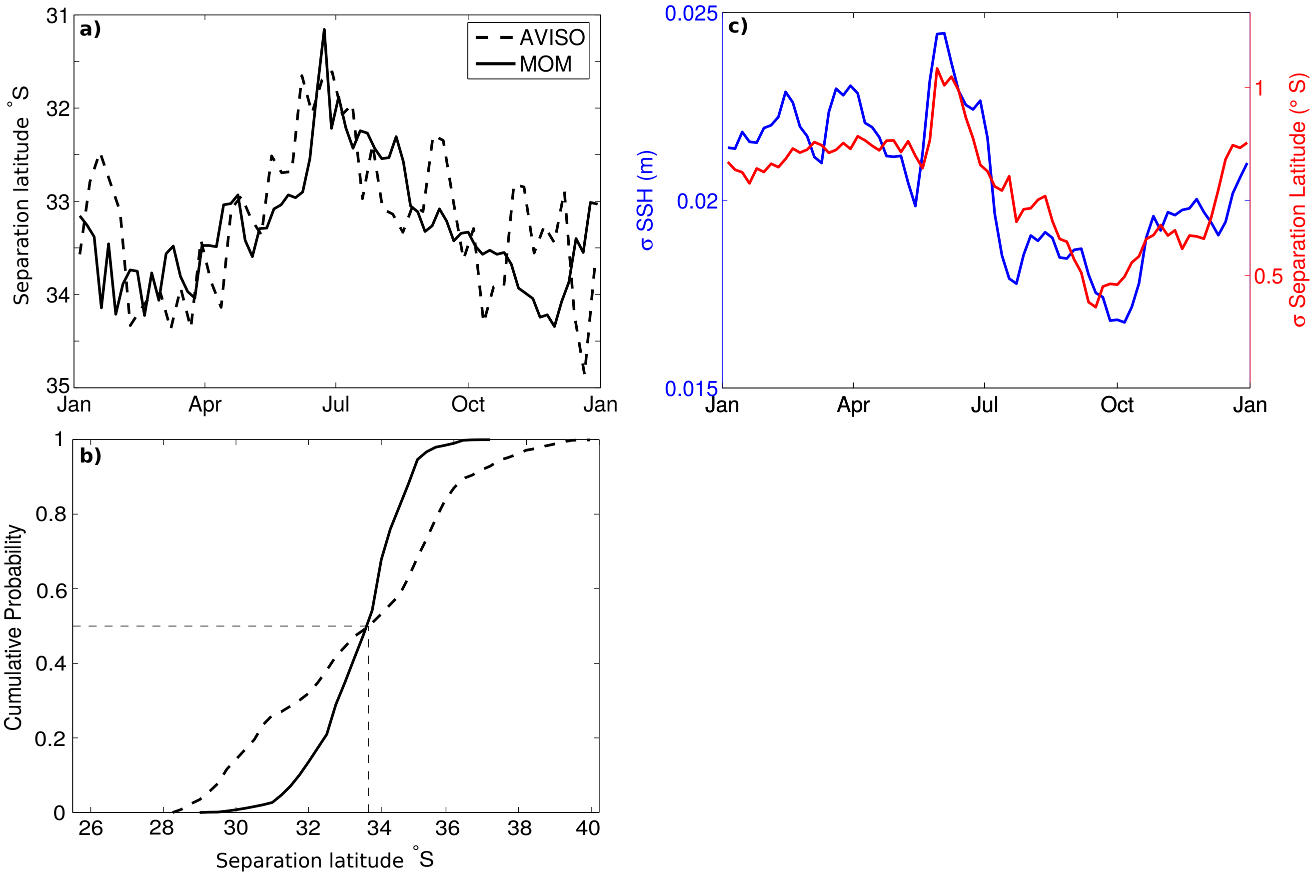

Figure 3. (a) Mean separation latitude and (b) Cumulative distribution function of the EAC separation latitude time series computed from the ocean model (solid line) and the AVISO data set (dashed line). The length of the time series used is 40 yrs and 19 yrs respectively. The median of the separation latitude of the MOM025 model output and the AVISO satellite altimetry is 33.6°S in both datasets. (c) Time series of the standard deviation of sea surface height (blue) and the separation latitude (red) of the ocean model, determined using a 55-day running mean. The average over 15 years is shown. Additionally, the standard deviation of the Sea Surface Height is averaged over the area between 20°S and 45°S and between 150°E and 160°E.

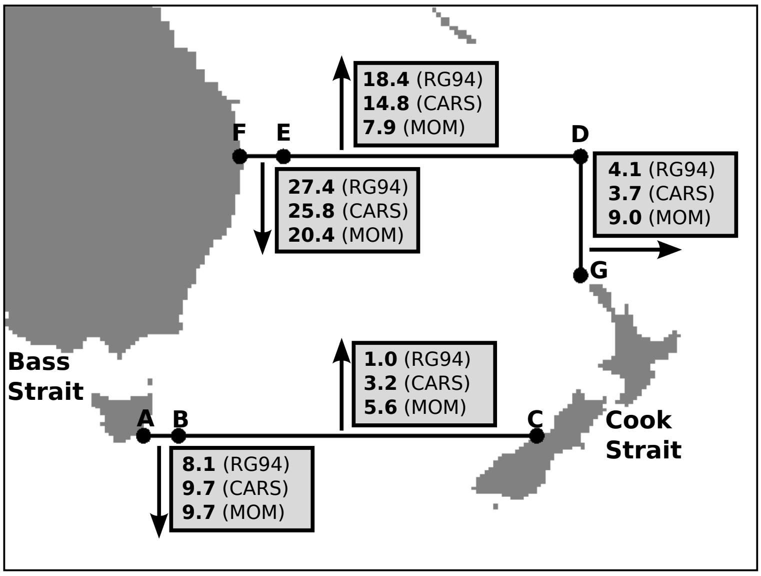

Figure 4. Mean net volume transport into and out of the Tasman Front. The numbers in the boxes indicate the transport (in Sv) in the direction of the corresponding arrow. The transports calculated by the model (MOM025) are compared to estimates from observations, *Ridgway and Godfrey* [1994] (RG94) and CARS, derived by *Oliver and Holbrook* [2014]. The sections are defined by the following locations: A (148°E, 43°S), B (150°E, 43°S), C (170.5°E, 43°S), D (173°E, 28°S), E (156°E, 28°S), F (153.5°E, 28°S) and G (173°E, 34.4°S).

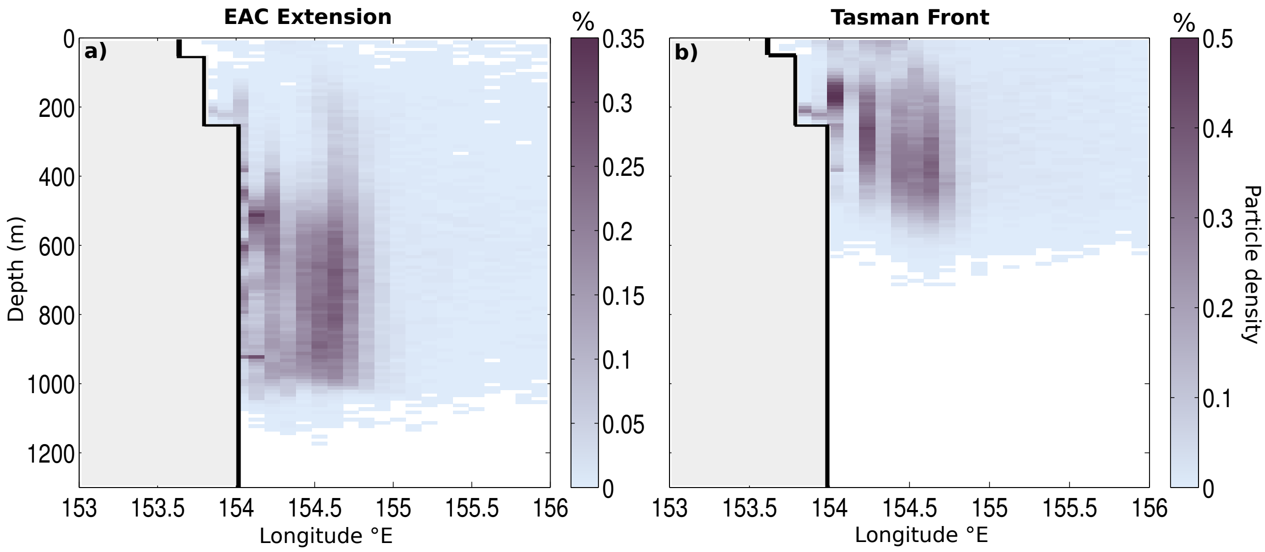

Figure 5. Depth profile at 28°S (transect shown in figure 1) upstream of the separation latitude of the particle density for particles following the extension of (a) the EAC and for (b) particles following the Tasman Front. The gray shading on the left side of the figures represents the bottom topography at this latitude.

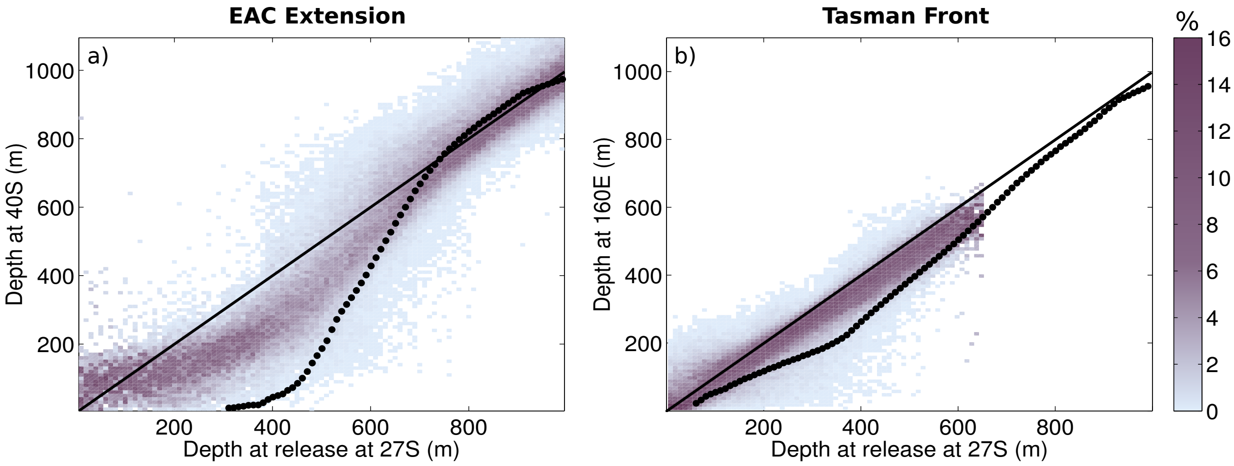

Figure 6. The distribution of the particles depth at transects after the separation (vertical axis) as a function of depth at which the particle originated from at 27°S (horizontal axis). The transects after the separation are chosen at 42°S and 160°E for the extension of the EAC and the Tasman Front, respectively. The black solid line represents y = x; high percentages coinciding with this line indicate that particles have not changed their depth. The distribution shown is calculated per depth interval of 10m thickness separately. The black dashed line represents the mean change in depth of isopycnals corresponding to the chosen transects.

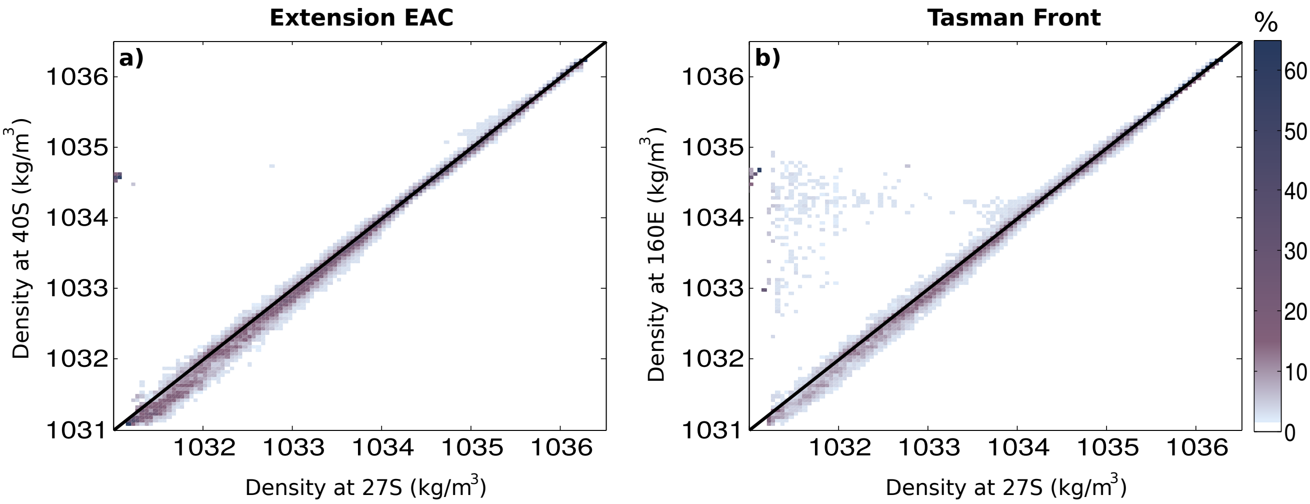

Figure 7. The distribution of the particles density at transects after the separation (vertical axis) as a function of the original density of the particle at 27°S (horizontal axis). The transects after the separation are chosen at 42°S and 160°E for the extension of the EAC and the Tasman Front, respectively. The black solid line represents y = x; high percentages coinciding with this line indicate that particles have not changed their density. The distribution shown is calculated per density interval of 0.05 kg/m^3 separately.

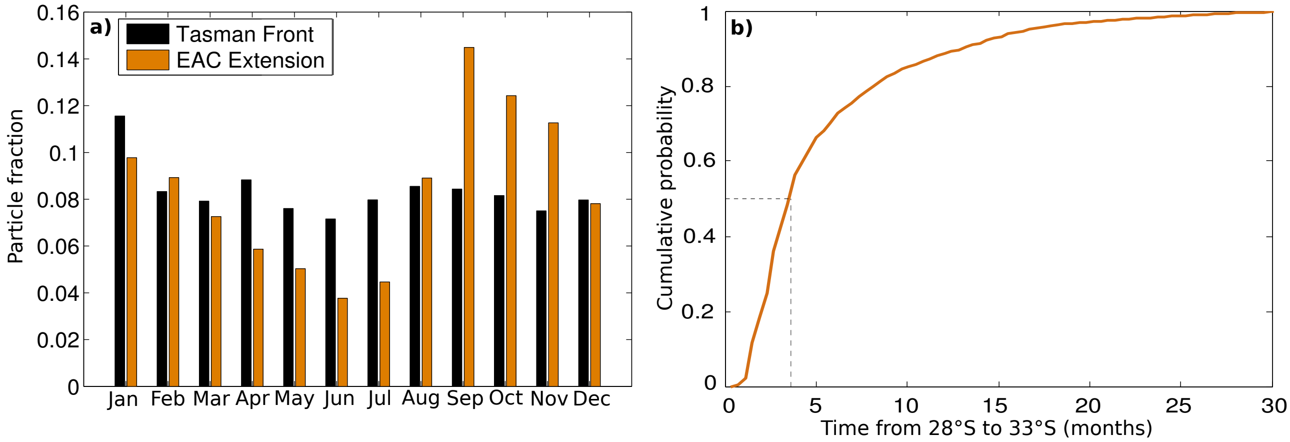

Figure 8. (a) Histogram of the time in the year when a particle crosses the transect at 28°S. The vertical axis shows the ratio between the number of particles crossing the transect in month X to the total number of particles following the specified pathway. (b) The cumulative probability of the transit time from 28°S to 33°, the mean separation latitude, for the particles following the EAC Extension crossing 28°S in September.

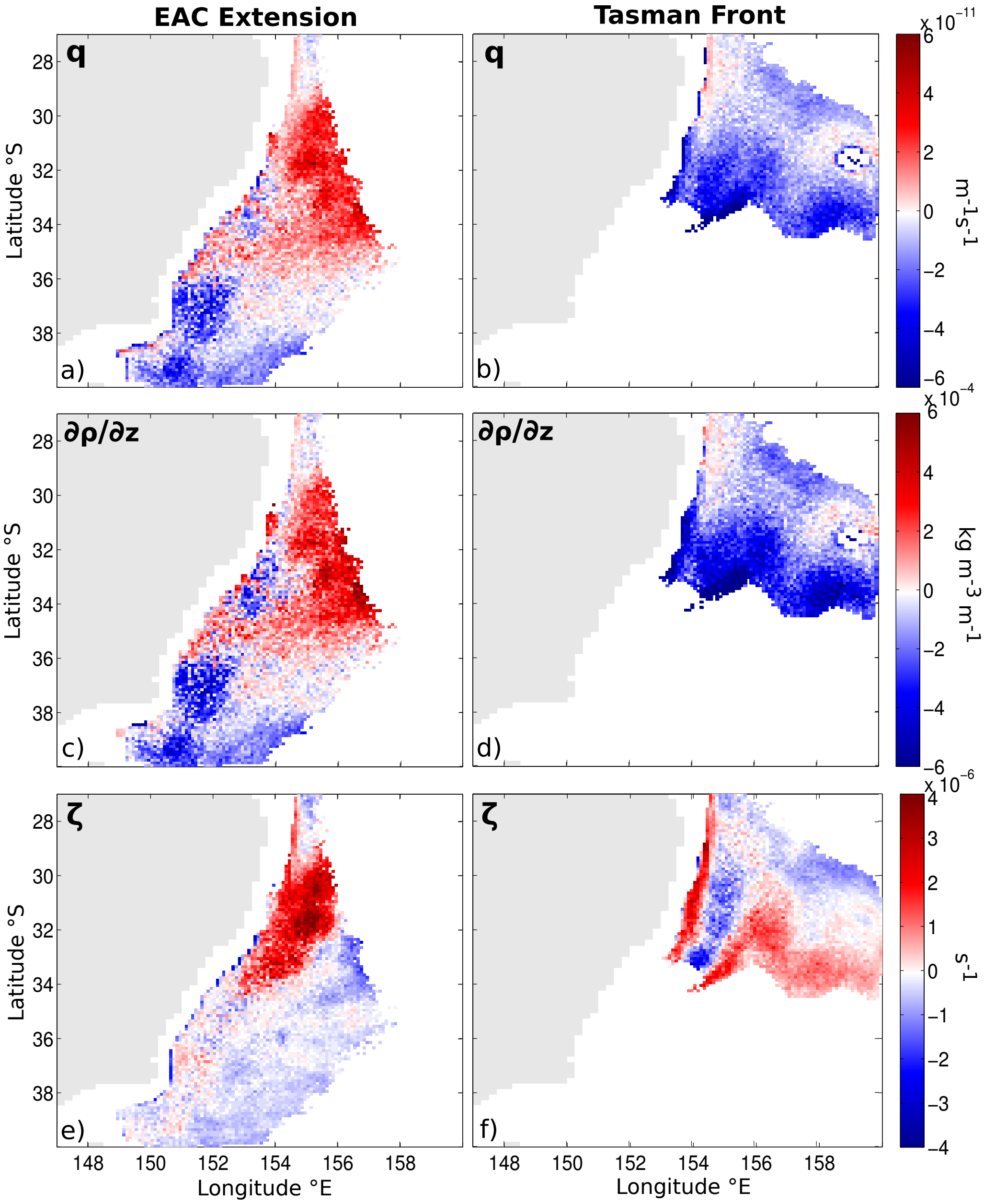

Figure 9. The anomaly for potential vorticity (q), the stratification ($\partial\rho/\partial z$) and relative vorticity (ζ) relative to the 15 year average of these terms for particles following the extension of the EAC (left column) and particles following the Tasman Front (right column). The anomalies are calculated from the mean of a random sample of 100 particles per grid box located between 350m and 450m depth where the two pathways overlap.

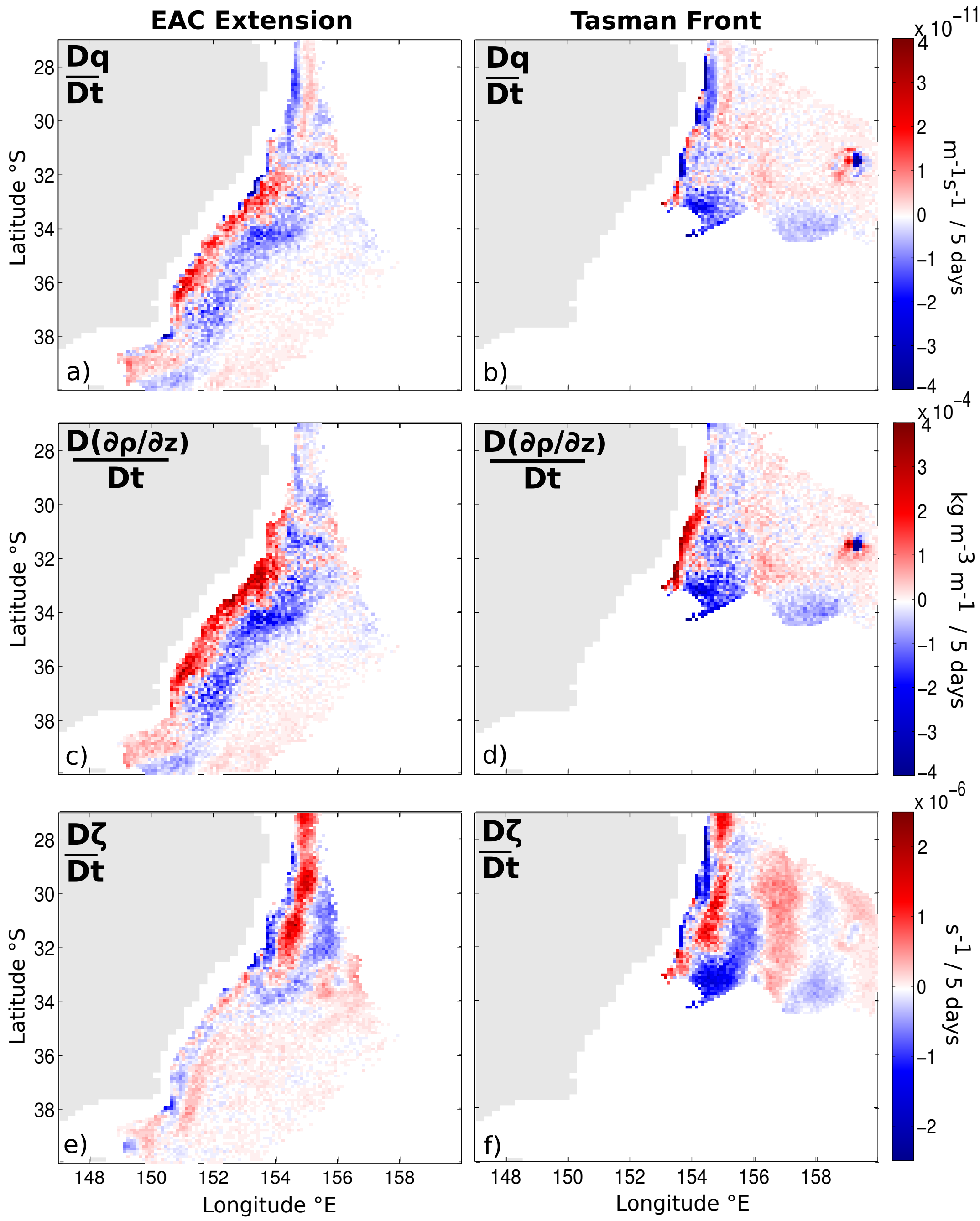

Figure 10. The material derivative of potential vorticity (q), the stratification ($\partial\rho/\partial z$) and relative vorticity (ζ) per 5 days, for particles following the extension of the EAC (left column) and particles following the Tasman Front (right column). The material derivative is calculated by using first-order differencing over a 5-day time window and is averaged over a random sample of 100 particles per grid box located between 350m and 450m depth.